Chinese Chemical Letters 33 (2022) 1917–1922

Contents lists available at ScienceDirect

Chinese Chemical Letters

journal homepage: www.elsevier.com/locate/cclet

Co-delivery of enzymes and photosensitizers *via* metal-phenolic network capsules for enhanced photodynamic therapy

Qian Wang[a], Zhiliang Gao[a], Kaijie Zhao[a], Peiyu Zhang[a], Qi-Zhi Zhong[a,b], Qun Yu[a,*], Shumei Zhai[a,*], Jiwei Cui[a,c]

[a] *Key Laboratory of Colloid and Interface Chemistry of the Ministry of Education, School of Chemistry and Chemical Engineering, Shandong University, Ji'nan 250100, China*
[b] *ARC Centre of Excellence in Convergent Bio-Nano Science and Technology, and the Department of Chemical Engineering, The University of Melbourne, Parkville, VIC 3010, United States*
[c] *State Key Laboratory of Microbial Technology, Shandong University, Qingdao 266237, China*

ARTICLE INFO

Article history:
Received 31 August 2021
Revised 10 November 2021
Accepted 12 November 2021
Available online 18 November 2021

Keywords:
Metal-phenolic network (MPN)
Photodynamic therapy (PDT)
Capsule
Oxygen self-supply
Drug delivery

ABSTRACT

The intrinsic hypoxic tumor microenvironment and limited accumulation of photosensitizers (PSs) result in unsatisfied efficiency of photodynamic therapy (PDT). To enhance the PDT efficiency against solid tumors, a functional oxygen self-supplying and PS-delivering nanosystem is fabricated *via* the combination of catalase (CAT), chlorin e6 (Ce6) and metal-phenolic network (MPN) capsule. It is demonstrated that the CAT encapsulated in the capsules (named CCM capsules) could catalyze the degradation of hydrogen peroxide (H_2O_2) to produce molecular oxygen (O_2), which could be converted into cytotoxicity reactive oxygen species (ROS) by surface-loaded Ce6 under 660 nm laser irradiation, leading to synergistic anticancer effects *in vitro* and *in vivo*. Therefore, the application of CCM capsule could be a promising strategy to improve PDT effectiveness.

Despite the rapid development of nanoparticle-based theranostic agents in cancer treatment, the clinical translation of nanomedicine still faces many challenges, such as poor efficacy, safety and scale-up/cost [1–3]. At present, the modulation of tumor microenvironments and the properties optimization of nanoparticles have been considered as efficient strategies to improve the therapeutic efficacy of cancer and facilitate the clinical translation of nanomedicine [4,5]. Photodynamic therapy (PDT), which employs photosensitizers (PSs) to generate ROS in the presence of oxygen (O_2) to kill cancer cells, is a major non-invasive strategy for superficial tumor treatment [6,7], due to its unique features, such as low side effects, high curative effects, and minimal invasiveness [8–10]. However, there still exist drawbacks that limit its clinical application. Firstly, the hydrophobic properties of most clinical PSs resulted in their aggregation under physiological conditions, limited tumor accumulation and reduction of the quantum yield of ROS production [11]. Secondly, the hypoxia in tumor reduces the PDT efficacy as it is an oxygen-dependent process [9,12]. Therefore, the development of strategies to overcome the shortcomings of PDT is of great significance for cancer therapy.

Recently, nanocarriers have been used to overcome some obstacles of PDT. For instance, nanocarriers with optimized properties have efficiently realized the tumor targeting delivery of PSs and O_2 [13–16]. What's more, based on the higher concentration of H_2O_2 in the tumor than normal tissues [17–19], *in situ* production of O_2 inside the tumor could be a more effective approach to overcome tumor hypoxia and enhance PDT [20]. For example, the use of catalase (CAT) to decompose the excessive H_2O_2 (ranging from 100 μmol/L to 1 mmol/L) for generation of O_2 is a promising approach to relieve the hypoxic tumor microenvironment and promote the therapeutic effect of PDT [21]. To date, the nanoparticulate system has been used for targeted delivery of functional enzymes with reduced off-target side effects [22]. However, compared with the methods of encapsulating enzymes inside or adsorbing on the surface of the nanoparticles, which could limit the loading efficiency and cause enzymes inactivation [23–25], enzyme encapsulation in a hollow capsule with a large cavity can maintain the enzyme's conformation freedom, and protect the encapsulated enzymes against degradation from exposure to the biological environment during blood circulation [26–28]. In particular, metal-phenolic network (MPN) capsules gained wide attention due to their unique properties, including facile assembly process, pH-responsive properties, lysosome escape ability, higher drug loading capacity, good biocompatibility and multifunctional imaging capability [27,29-35].

* Corresponding authors.
E-mail addresses: qunyu@sdu.edu.cn (Q. Yu), smzhai@sdu.edu.cn (S. Zhai).

https://doi.org/10.1016/j.cclet.2021.11.040
1001-8417/

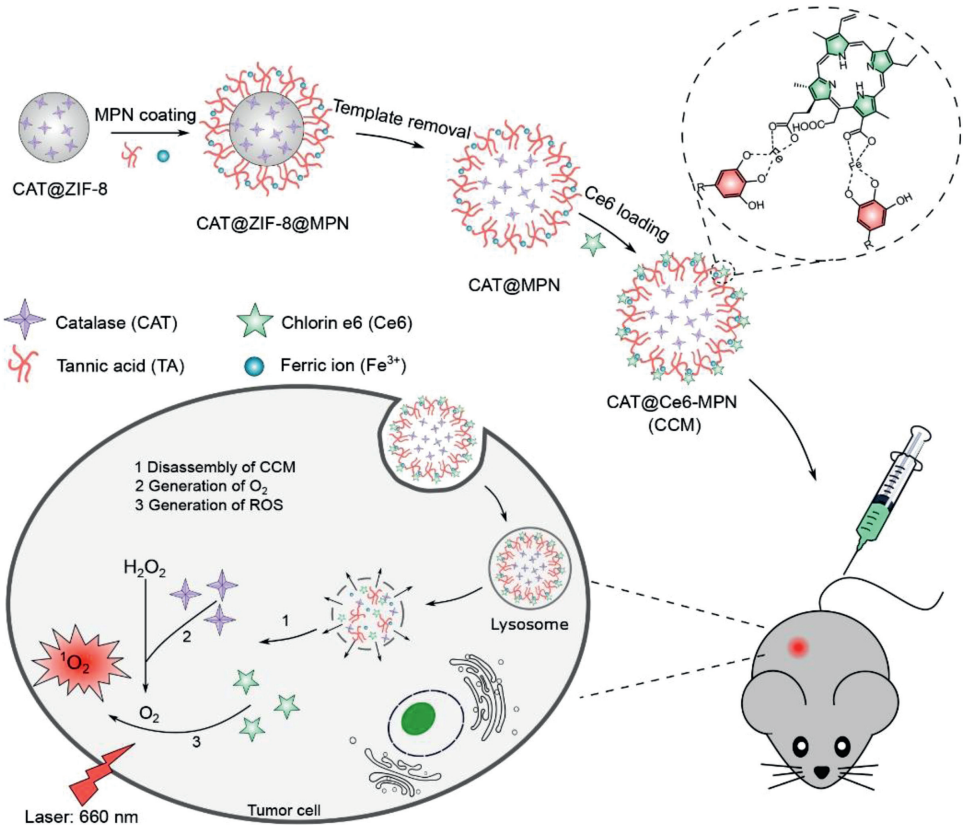

Fig. 1. Schematic illustration of CCM capsule preparation and the mechanism involved in PDT enhancement against cancer.

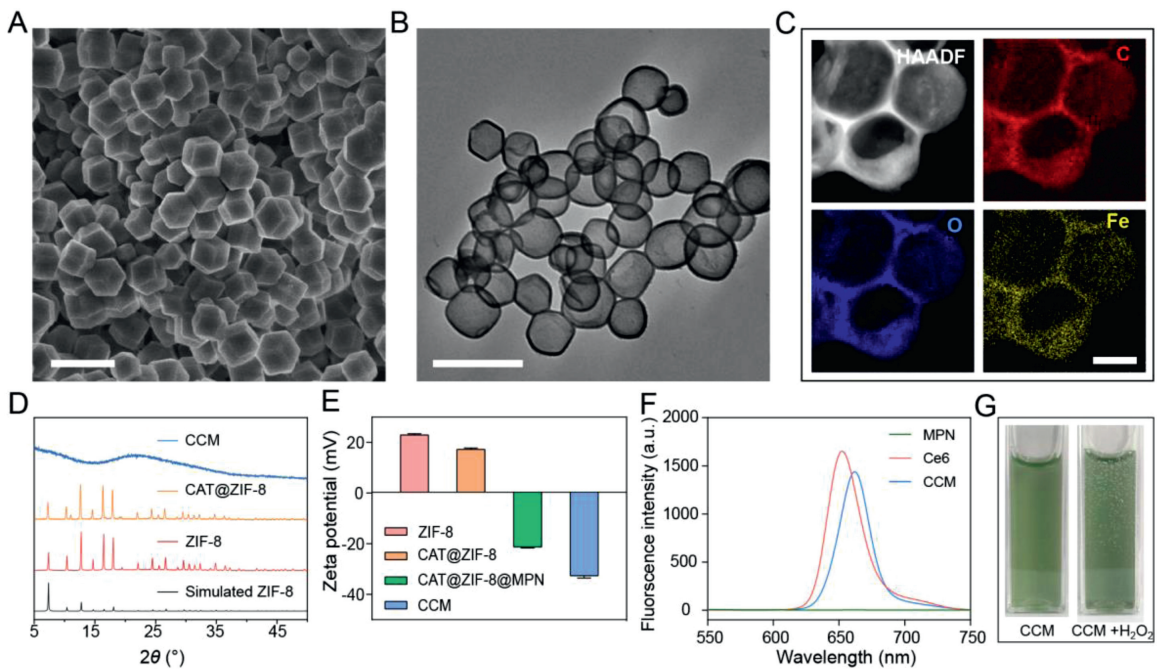

Fig. 2. Characterization of CAT@ZIF-8 NPs and CCM capsules. (A) SEM image of CAT@ZIF-8 NPs. (B) TEM image of CCM capsules. Scale bars are 500 nm. (C) HAADF-STEM and EDX mapping images of CCM capsules, showing carbon (C), oxygen (O), and iron (Fe) elements. The scale bar is 100 nm. (D) PXRD patterns of CCM, CAT@ZIF-8 NPs, ZIF-8 NPs and simulated ZIF-8. (E) Zeta potential of ZIF-8 NPs, CAT@ZIF-8 NPs, CAT@ZIF-8@MPN NPs, and CCM capsules in water. Data are represented as the means ± SD, $n = 3$. (F) Fluorescence spectra of MPN capsules, free Ce6, and CCM capsules. (G) Optical photograph of CCM capsule suspension without/with 100 mmol/L H_2O_2.

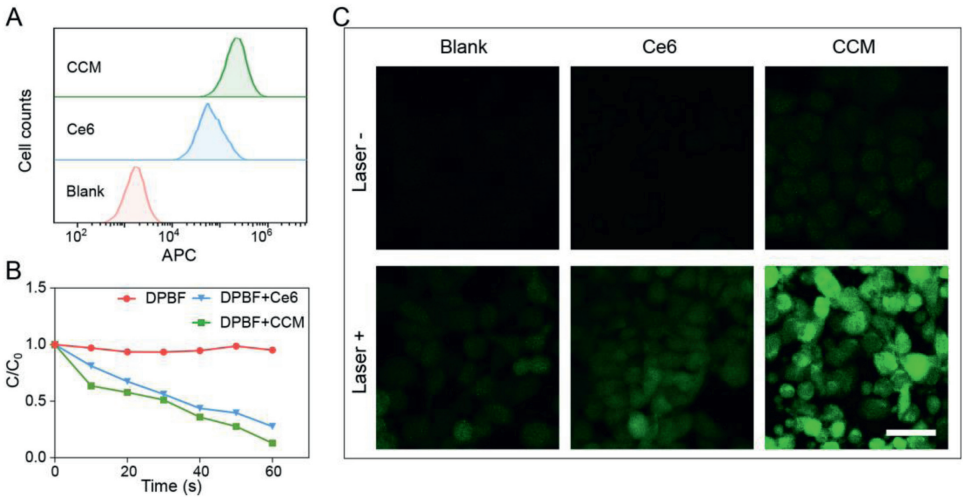

Fig. 3. (A) Flow cytometry analysis of 4T1 cells treated with free Ce6 or CCM capsules for 2 h. (B) Normalized concentration of the DPBF in the presence of free Ce6 or CCM capsules. (C) CLSM images showing the production of ROS detected by DCFH-DA. The scale bar is 50 μm.

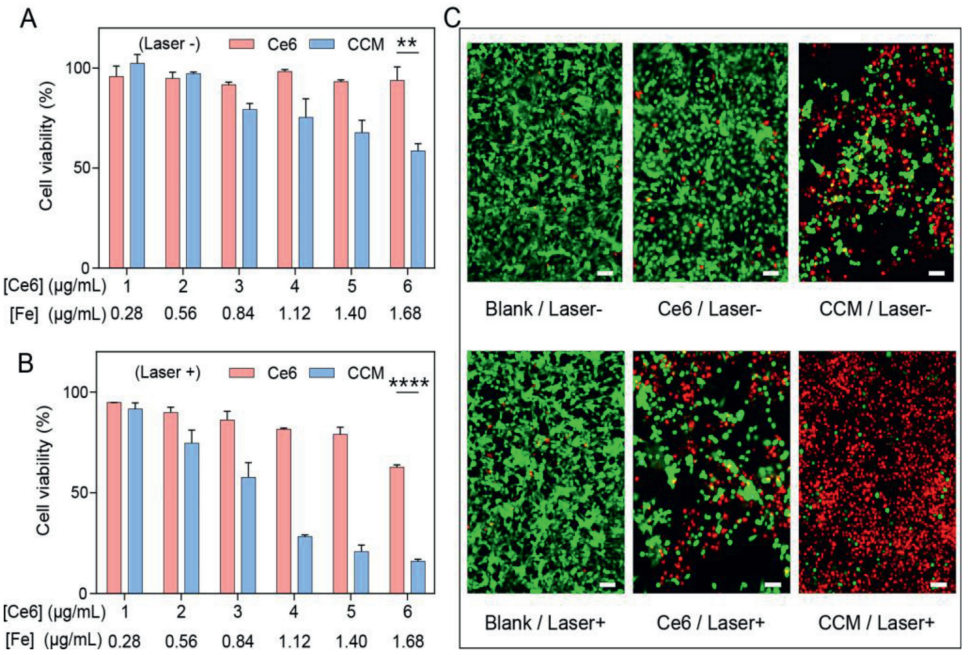

Fig. 4. Viability of 4T1 cells after incubation with different concentrations of free Ce6 or CCM capsules (A) without or (B) with irradiation by 660 nm laser for 1 min. Data are represented as the means ± SD, $n = 3$, $^{**}P < 0.01$, $^{****}P < 0.001$. (C) Fluorescence images of live/dead cells after treatment with free Ce6 and CCM capsules with/without irradiation. Green fluorescence represents live cells and red fluorescence represents dead cells. Scale bars are 50 μm.

Herein, we constructed a high-performance PDT nanosystem (denoted as CCM capsules) *via* a facile and biofriendly strategy. In our system, CAT-loading MPN capsules were prepared by zeolite imidazolate frameworks (ZIF-8) sacrifice templating method, where ZIF-8 encapsulated CAT *via* biomimetic mineralization followed by coating with tannic acid (TA) and Fe^{3+}. Subsequently, chlorin e6 (Ce6) was loaded onto the capsules through the coordination between carboxyl group (-COOH) and Fe^{3+} (Fig. 1). This nanosystem could significantly improve the PDT efficacy through overcoming the hypoxia in tumor microenvironment and increasing the accumulation of Ce6 in tumor.

To encapsulate CAT into ZIF-8 NPs, CAT and 8-arm poly(ethylene glycol) (8-arm-PEG-OH) were mixed with zinc nitrate and 2-methylimidazole (2-MIM) in an aqueous solution. The 8-arm-PEG-OH can extract Zn^{2+} due to the interactions between the repeat unit of ethoxyl groups in PEG and Zn^{2+}, and induce the mineralization of Zn^{2+} with 2-MIM and CAT [36–38]. Then, MPN films were easily deposited on the surface of the CAT@ZIF-8 NPs based on the high adhesion between tannic acid (TA) with substrates and the strong coordinating ability of TA with Fe^{3+} [39]. Finally, ethylenediaminetetraacetic acid disodium salt (EDTA) was used to remove the ZIF-8 NPs followed by the cooperation of Ce6 to obtain the hollow CCM capsules containing CAT and Ce6. Scanning electron microscopy (SEM) (Fig. 2A) and transmission electron microscopy (TEM) images (Fig. S1A in Supporting information) showed that the CAT@ZIF-8 NPs have a dodecahedral morphology with a size of about 250 nm, which is similar to ZIF-8 NPs (Figs. S1B and C in Supporting information). Energy-dispersive X-ray (EDX) mapping analysis of CCM capsules showed the well-matched elements (C, O, and Fe) distribution (Figs. 2B and C). The patterns of ZIF-8 NPs powder X-ray diffraction (PXRD) and CAT@ZIF-8 NPs matched well with the simulated one (Fig. 2D), which indicated that the encapsulation of CAT did not affect the crystal structure of ZIF-8 NPs. The hollow and

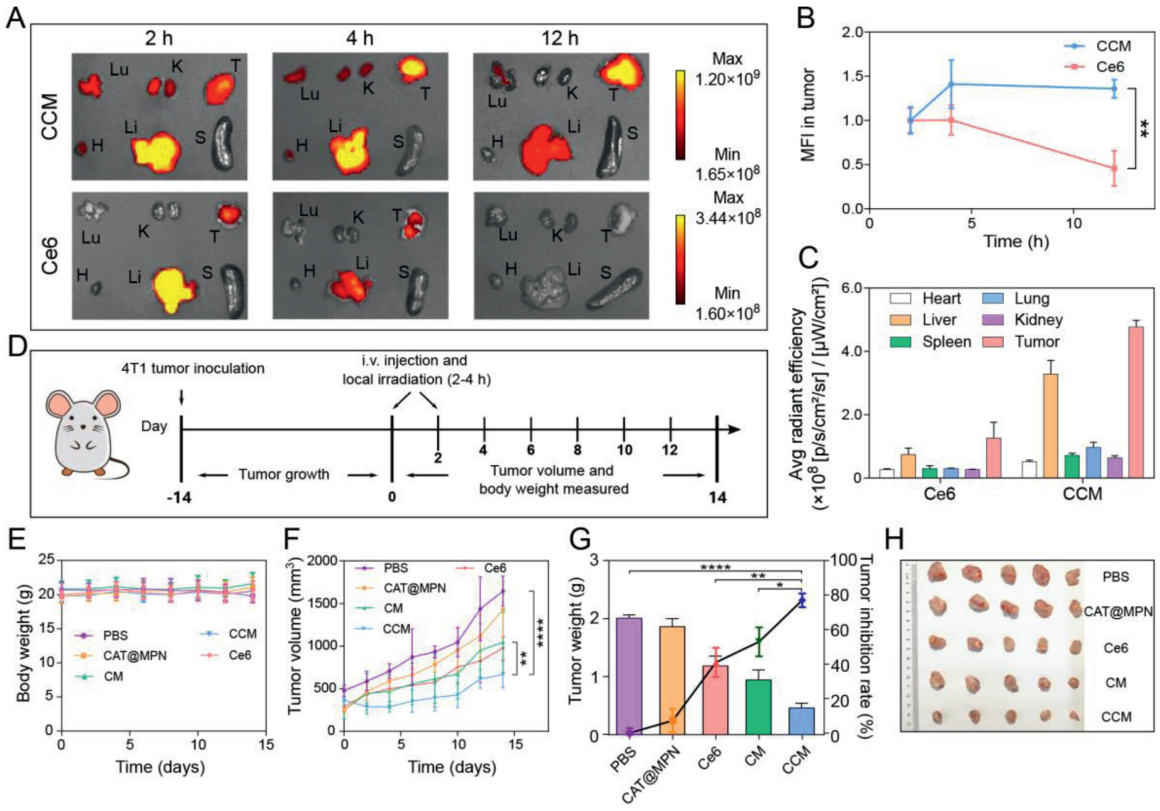

Fig. 5. The biodistribution and antitumor properties of CCM capsules towards 4T1 tumor-bearing Balb/c mice. (A) *Ex vivo* fluorescence images of major organs and tumors excised from mice at 2, 4 and 12 h after intravenous injection of CCM capsules or free Ce6. Lu, K, T, H, Li, and S stand for lung, kidneys, tumor, heart, liver and spleen, respectively. (B) Relative mean fluorescence intensity of tumors. Data are represented as the means ± SD, $n = 3$. (C) Average radiant efficiency of the isolated organs and tumors at 12 h after intravenous injection of free Ce6 and CCM capsules. Data are represented as the means ± SD, $n = 3$. (D) A schematic diagram of the inoculation and treatment protocol of 4T1 subcutaneous tumor. (E) Time-dependent variations of body weight, and (F) tumor volume. Data are represented as the means ± SD, $n = 5$. (G) Tumor weight and corresponding tumor inhibition rate. Data are represented as the means ± SD, $n = 5$. (H) The photograph of the excised tumors. $^{*}P < 0.05$, $^{**}P < 0.01$, $^{****}P < 0.0001$.

amorphous structure of CCM capsules supported the successful removal of ZIF-8 NPs [23,40,41]. As shown in Fig. 2E, the change of zeta potential values from 22.6 mV to 17.7 mV for ZIF-8 NPs and CAT@ZIF-8 NPs indicated the successful encapsulation of CAT. After MPN films were deposited and the templates were removed, zeta potential values become –21.5 and –33.2 mV respectively. When CCM capsules were dispersed in RPMI 1640 medium, the zeta potential value changed to be −17.2 mV compared to that (–33.2 mV) in water [36], which could be due to the adsorption of protein corona on CCM capsules. Meanwhile, the specific absorption peaks of Ce6 (about 660 nm) and ligand-metal charge transfer band of phenol-iron coordination (500–650 nm) can be detected in the ultraviolet-visible spectroscopy (UV–vis) [42], indicating the successful fabrication of CCM capsules (Fig. S2 in Supporting information). In addition, the emission peak of the fluorescence spectrum around 670 nm also confirmed the successful loading of Ce6 in CCM capsules (Fig. 2F). The loading efficiency of Ce6 in CCM capsules was about 11.7% based on the standard curve of Ce6 (Figs. S3A and B in Supporting information). The loading efficiency of CAT in CAT@ZIF-8 NPs was about 95.87% (230.1 U/mg) based on the standard curve of CAT (Fig. S4 in Supporting information). The catalytic activity of CAT was evaluated *in vitro*. As shown in Fig. 2G and Fig. S5 (Supporting information), due to the permeability of the capsules [29,43], obvious bubbles were generated in CCM and CAT@MPN capsule suspensions after adding of H_2O_2 solution, which was not observed in Ce6@MPN (CM) or MPN capsule suspensions. These results indicated that CAT loaded CCM capsules could effectively decompose H_2O_2 into O_2, which was expected to improve the oxygen level in hypoxic tumors microenvironment.

To investigate the cell uptake of CCM, 4T1 cells were incubated with Ce6 or CCM capsules for different periods (0.5, 1, and 2 h) followed by flow cytometry analysis. The result showed that more Ce6 and CCM capsules were associated with 4T1 cells with the increase of incubation time (Fig. S6 in Supporting information), indicating the time-dependent cellular uptake. In addition, higher levels of Ce6 signal were observed in cells treated with CCM capsules than those treated with free Ce6, suggesting the increased delivery of Ce6 by CCM capsules (Fig. 3A). The enhanced cellular uptake of Ce6 by CCM was confirmed by confocal laser scanning microscope (CLSM) (Fig. S7 in Supporting information). After incubation for 2 h, red fluorescence of Ce6 could be observed inside the 4T1 cells and the fluorescence signal in cells treated with CCM capsules was much stronger than those treated with free Ce6.

Under a specific wavelength (660 nm), the energy transfer from excited Ce6 to the surrounding oxygen leads to the production of high cytotoxic ROS [44]. In this study, 1,3-diphenylisobenzofuran (DPBF) was used as a probe to detect the generation of ROS *in vitro* [45–47]. As shown in Fig. 3B, normalized change in concentration of DPBF in the presence of CCM capsules is similar to that in the presence of Ce6 under 660 nm laser irradiation, demonstrating the same efficiency of ROS generation. In addition, DCFH-DA was used as a fluorescence probe to detect the intracellular ROS level *via* flow cytometry and CLSM [47,48]. As shown in Fig. S8 (Supporting information), 4T1 cells incubated with CCM capsules plus laser irradiation displayed the highest fluorescence intensity compared to those incubated with free Ce6, indicating the enhanced Ce6 cellular internalization through CCM capsules. The generation of ROS was further confirmed by CLSM (Fig. 3C). Without laser ir-

radiation, weak fluorescence signals were observed in cells treated with free Ce6 or CCM capsules, in contrast, laser irradiation induced the strongest green fluorescence in cells treated with CCM capsules, indicating efficient generation of ROS.

To investigate the potential anticancer activity of CCM capsules, the cytotoxicity of CCM capsules were measured in 4T1 cells by MTT method and live/dead assay. As shown in Fig. 4A and Fig. S9A (Supporting information), free Ce6, MPN, and CM capsules did not exhibit obvious cytotoxicity without 660 nm laser irradiation, while CAT@MPN and CCM capsules exhibited cytotoxicity in a concentration-dependent manner, which can be ascribed to the disruption of redox balance in cells induced by CAT [49]. Upon a 660 nm laser irradiation, the CCM capsules showed the highest cytotoxicity (Fig. 4B and Fig. S9B in Supporting information). Moreover, live/dead cell fluorescent staining assay showed that CCM capsules plus laser irradiation killed 4T1 cells more effectively than other treatments (Fig. 4C and Fig. S10 in Supporting information).

To visually detect the biodistribution of CCM capsules *in vivo*, free Ce6 and CCM capsules were intravenously injected into the 4T1 tumor-bearing Balb/c female mice, and the *in vivo* fluorescence signals were monitored at predetermined time points (Fig. S11 in Supporting information). The result showed that a relatively weak fluorescence signal was detected in tumor site of mice treated with free Ce6 (Figs. 5A and B). The fluorescence signal decreased along with time and no obvious fluorescence was observed after 12 h, indicating that free Ce6 could be quickly excreted from the body (Fig. 5C) [15]. In contrast, a much stronger fluorescence signal was observed at the tumor site of mice treated with CCM capsules (Figs. 5A and B). Compared with the other organs, the tumors were found to show a high average radiant efficacy after 12 h, which was probably due to the EPR effect (Fig. 5C). These results illustrated that CCM capsules could increase accumulation of Ce6 in the tumor and provide a possible platform for further antitumor application *in vivo*.

To evaluate the antitumor effects of CCM capsules, 4T1 tumor-bearing female mice were divided into five groups and exposed to PBS, CAT@MPN, free Ce6, CM and CCM capsules as indicated (Fig. 5D). Intravenous injection of CAT@MPN capsules did not significantly inhibit tumor growth (Fig. 5F). The free Ce6 and CM capsules plus 660 nm laser irradiation inhibited the growth of tumor to some extent due to the basic PDT therapeutic efficacy. In contrast, CCM capsules treatment plus 660 nm laser irradiation significantly suppressed the tumor growth, which could be attributed to the effective accumulation of Ce6 and the generation of ROS in tumor (Fig. 5F). At the end of day 14, CCM capsules treatment plus laser irradiation resulted in the lowest tumor weight (0.45 g) and the highest tumor inhibition rate of 77.1% (Fig. 5G). The volume of tumors in the group of CCM capsules treatment was the smallest among all tumors (Fig. 5H). During the entire treatment period, no changes of body weights (Fig. 5E) and abnormal behaviors were observed, indicating the low side effects of CCM capsules. All animal procedures were performed in accordance with the Guidelines for Care and Use of Laboratory Animals of Shandong University and approved by the Animal Ethics Committee of Shandong University.

In summary, we reported the design and fabrication of a novel nanosystem, named CCM capsules, through the combination of CAT, Ce6 and MPN capsules to enhance the efficacy of PDT. We proved that CCM capsules possess a good capability to decompose H_2O_2 to generate O_2, thus effectively alleviating the hypoxic microenvironment of tumor. The photosensitizer Ce6 loaded on MPN capsules by cooperating with iron ions could be efficiently delivered into tumor tissues *in vitro* and *in vivo*. Therefore, the novel nanosystem has the potential to become a promising platform for enhancement of PDT and other oxygen-dependent tumor therapy.

Declaration of competing interest

The authors declare that they have no known competing financial interests or personal relationships that could have appeared to influence the work reported in this paper.

Acknowledgments

This work was supported by the Innovation Project of Jinan Science and Technology Bureau (No. 2020GXRC022), the Project for Scientific Research Innovation Team of Young Scholar in Colleges and Universities of Shandong Province (No. 2020KJC001) and the National Natural Science Foundation of China (No. 21677090). This work was performed in part at the Translational Medicine Core Facility of Advanced Medical Research Institute at Shandong University.

Supplementary materials

Supplementary material associated with this article can be found, in the online version, at doi:10.1016/j.cclet.2021.11.040.

References

[1] Y. Min, J.M. Caster, M.J. Eblan, et al., Chem. Rev. 115 (2015) 11147–11190.
[2] C. Zheng, M. Li, J. Ding, BIO Integration 2 (2021) 57–60.
[3] C.Y. Zhang, L. Yan, X. Wang, et al., Nano Today 35 (2020) 101008.
[4] J.X. Ding, J.J. Chen, L.Q. Gao, et al., Nano Today 29 (2019) 100800.
[5] M.J. Mitchell, M.M. Billingsley, R.M. Haley, et al., Nat. Rev. Drug Discov. 20 (2021) 101–124.
[6] X. Chen, Z. Yi, G. Chen, et al., ACS Sustain. Chem. Eng. 8 (2020) 16372–16384.
[7] J. Wang, H. Wu, Y. Yang, et al., Nanoscale 10 (2018) 132–141.
[8] X. Li, S. Lee, J. Yoon, Chem. Soc. Rev. 47 (2018) 1174–1188.
[9] Z. Zhou, J. Song, L. Nie, et al., Chem. Soc. Rev. 45 (2016) 6597–6626.
[10] B. Yang, Y. Chen, J. Shi, Chem. Rev. 119 (2019) 4881–4985.
[11] X.S. Wang, J.Y. Zeng, M.K. Zhang, et al., Adv. Funct. Mater. 28 (2018) 1801783.
[12] G. Yang, L. Xu, J. Xu, et al., Nano Lett. 18 (2018) 2475–2484.
[13] Z. Zhang, W. Sang, L. Xie, et al., Angew. Chem. Int. Ed. 60 (2021) 1967–1975.
[14] J. Wei, J. Li, D. Sun, et al., Adv. Funct. Mater. 28 (2018) 1706310.
[15] S.Z.F. Phua, G. Yang, W.Q. Lim, et al., ACS Nano 13 (2019) 4742–4751.
[16] H. Fang, Y. Gai, S. Wang, et al., J. Nanobiotechnology 19 (2021) 81.
[17] T.P. Szatrowski, C.F. Nathan, Cancer Res. 51 (1991) 794–798.
[18] Y. Kuang, K. Baakrishnan, V. Gandhi, et al., J. Am. Chem. Soc. 133 (2011) 19278–19281.
[19] J. Kim, H.R. Cho, H. Jeon, et al., J. Am. Chem. Soc. 139 (2017) 10992–10995.
[20] N. Yang, W.Y. Xiao, X.J. Song, et al., Nano-Micro Lett. 12 (2020) 27.
[21] A.Y. Heble, J. Santelli, A.M. Armstrong, et al., ACS Appl. Mater. Interfaces 13 (2021) 5945–5954.
[22] S. Jiang, Y. Zhang, Y. Yang, et al., ACS Appl. Mater. Interfaces 11 (2019) 10554–10558.
[23] X. Ma, H. Sui, Q. Yu, et al., Langmuir 37 (2021) 3166–3172.
[24] H. An, M. Li, J. Ga, et al., Coord. Chem. Rev. 384 (2019) 90–106.
[25] H. Zhang, J. Luo, S. Li, et al., Langmuir 34 (2018) 2585–2594.
[26] F.P. Chang, Y. Hung, J.H. Chang, et al., ACS Appl. Mater. Interfaces 6 (2014) 6883–6890.
[27] Q. Huo, J. Zhao, W. Li, et al., Chem. Comm. 55 (2019) 7155–7158.
[28] M. Li, S. Qiao, Y. Zheng, et al., J. Am. Chem. Soc. 142 (2020) 6675–6681.
[29] H. Ejima, J.J. Richardson, K. Liang, et al., Science 341 (2013) 154–157.
[30] X. Zhang, Z. Li, P. Yang, et al., Mater. Horizons 8 (2021) 145–167.
[31] J. Guo, Y. Ping, H. Ejima, et al., Angew. Chem. Int. Ed. 53 (2014) 5546–5551.
[32] G. Yun, Q.A. Besford, S.T. Johnston, et al., Chem. Mater. 30 (2018) 5750–5758.
[33] Q. Wang, Z. Gao, Q.Z. Zhong, et al., Langmuir 37 (2021) 11292–11300.
[34] Q.Z. Zhong, J.J. Richardson, S. Li, et al., Angew. Chem. Int. Ed. 59 (2020) 1711–1717.
[35] Q.Z. Zhong, S. Li, J. Chen, et al., Angew. Chem. Int. Ed. 58 (2019) 12563–12568.
[36] Q. Yu, Y. Tian, M. Li, et al., Chem. Comm. 56 (2020) 11078–11081.
[37] A. Hamta, M.R. Dehghani, J. Mol. Liq. 231 (2017) 20–24.
[38] G. Zhang, X. Fu, H. Sun, et al., ACS Appl. Mater. Interfaces 13 (2021) 13978–13989.
[39] H. Ejima, J.J. Richardson, F. Caruso, Nano Today 12 (2017) 136–148.
[40] M.A. Rahim, K. Kempe, M. Muellner, et al., Chem. Mater. 27 (2015) 5825–5832.
[41] C. Yang, J. Xu, D. Yang, et al., Chin. Chem. Lett. 29 (2018) 1421–1424.
[42] M.A. Rahim, H. Ejima, K.L. Cho, et al., Chem. Mater. 26 (2014) 1645–1653.
[43] J. Chen, S. Pan, J. Zhou, et al., Chem. Mater. 32 (2020) 6975–6982.
[44] M. Chen, Y. Zhang, L. Cui, et al., Chem. Eng. J. 422 (2021) 130089.

[45] B. Ding, S. Shao, C. Yu, et al., Adv. Mater. 30 (2018) 1802479.
[46] K. Zhang, X. Meng, Y. Cao, et al., Adv. Funct. Mater. 28 (2018) 1804634.
[47] Z. Gao, T. He, P. Zhang, et al., ACS Appl. Mater. Interfaces 12 (2020) 20271–20280.
[48] P. Zhang, Z. Gao, J. Cui, et al., ACS Appl. Bio. Mater. 3 (2020) 561–569.
[49] C.C. Huang, W.T. Chia, M.F. Chung, et al., J. Am. Chem. Soc. 138 (2016) 5222–5225.